SIAM J. SCI. COMPUT.
Vol. 16, No. 4, pp. 755–772, July 1995

001

A FRONT TRACKING METHOD FOR COMPRESSIBLE FLAMES IN ONE DIMENSION*

JAMES HILDITCH† AND PHILLIP COLELLA†

Abstract. A numerical method is presented for the treatment of one-dimensional compressible flames. The method consists of a conservative front tracking algorithm for use near the flame and a high-order finite difference scheme for capturing the hydrodynamics throughout the rest of the domain. The results presented show that the method effectively models the interaction of gas dynamics with both deflagration and detonation waves. This approach has the advantage that it can be generalized to more than one dimension.

Key words. front tracking, compressible flow, combustion, conservation laws

AMS subject classifications. 65M06, 80.08, 76N10, 35L65

Notation

c	speed of sound	u	velocity
e	internal energy	U	vector of conserved quantities
E	total energy	W	mass flux through a discontinuity
F	vector of fluxes	x	position
i	finite difference cell label	α	eigenvector expansion coefficient
k	flame speed constant	γ	ratio of specific heats
l_k	kth left eigenvector	Γ^-	- Riemann invariant
n	finite difference time step label	δ	flame thickness
P	pressure	δM	reduced mass
q	chemical energy	ΔH_R	heat of reaction
Q	flame speed constant	$\Delta t, \Delta x$	finite difference time step, grid spacing
r	finite difference stencil width	λ	eigenvalue
r_k	kth right eigenvector	Λ	volume fraction (length fraction in one dimension)
s, S	front speed, flame speed	ρ	density
t	time	τ	specific volume
T	temperature		

subscripts and superscripts

CJ	Chapman–Jouguet	tot	total quantity
f	flame, front	$-, +$ (sup)	$-, +$ eigenmode
k	eigenmode $-, 0\rho, 0q, +$	0	state ahead of a deflagration
L, R	left (behind), right (in front of) the tracked front	1,2	states in front of and behind gas wave
S	dummy value representing L or R	$*$	state inside Riemann solution wave pattern

1. Introduction.

There are two principal approaches for the treatment of discontinuities in high-resolution numerical solutions of hyperbolic conservation laws. The first, front capturing, represents discontinuities as steep gradients resolved over a small number of finite difference cells. This method typically employs diffusion terms — either introduced by the truncation error in the method or by an explicit viscous term — to suppress numerical oscillations near the discontinuity. In front tracking, the discontinuity is treated as an internal boundary in the flow field (see [17] for a survey). The behavior of the tracked front is governed by the Rankine–Hugoniot relations and appropriate entropy conditions. Away from the front, a higher-order finite difference scheme is used to update the solution in time. The combination

*Received by the editors May 26, 1993; accepted for publication (in revised form) April 18, 1994.

†Mechanical Engineering Department, University of California, Berkeley, California 94720 (jim@bigbird.berkeley.edu, pcolella@euler.berkeley.edu). Research supported at University of California Berkeley by Defense Advanced Research Projects Agency (DARPA) and National Science Foundation grant DMS-8919074, National Science Foundation Presidential Young Investigator award grant ACS-8958522; and Department of Energy High Performance Computing and Communications Program grant DE-FGO3-92ER25140. The first author was supported by a National Science Foundation graduate fellowship.

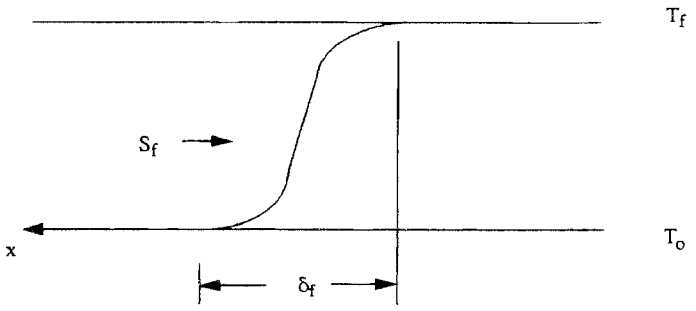

FIG. 1. *Premixed flame.*

of front tracking and high-resolution finite difference methods produces a globally conservative method that has proven successful in several applications including multidimensional modelling of high Mach number gas dynamics and modelling of combustion systems in the incompressible regime (see [11], [16], [22]).

An application that yields itself to analysis using front tracking is the study of deflagration and detonation waves in a compressible flow field. There has been much work in the area of front tracking applied to detonations (see, e.g., [3], [5], [7], [8]) but little in the area of compressible flames. In [19] both deflagrations and detonations in one dimension were tracked using a moving mesh method. Extension of their work to multiple space dimensions, however, is nontrivial. Although the approach outlined here is applied to a one-dimensional reacting flow, the method may be generalized to multiple dimensions. Our approach uses a volume of fluid tracking method that has the ability to effectively represent large deformations, changes in the topology of the front, and complex geometries [4], [21]. When applied in that context, the Riemann solution may be modified to include more complex physical phenomena such as curvature effects [6]. We will not comment further on these except to say that the current formulation does not restrict computation to one dimension.

Physically, the scenario to be modelled is a combustion wave travelling through a one-dimensional premixed reacting medium. If one assumes the combustion wave to be infinitely thin, the front tracking method can be used to handle the reacting front. The numerical scheme maintains a sharp discontinuity at the flame: however, since we do not compute the internal structure of the flame resulting from diffusional effects and finite rate chemistry, the flame speed must now be modelled.

This paper demonstrates the successful application of the front tracking algorithm to systems of hyperbolic conservation laws for reacting gas flow. The present focus is not on understanding the mechanisms of transition from deflagration to detonation or on the validation of empirical flame speed laws, but rather on formalizing the procedure necessary to implement the algorithm so that future studies might yield physically instructive results.

2. Problem description and modelling considerations.

Physical problem. Consider the propagation of a reacting front through a one-dimensional premixed medium (see, e.g., [18], [24]). In general, the upstream conditions (pressure, temperature, velocity, reactant concentrations) are known and one is interested in determining the flame speed and downstream conditions. For example, in Fig. 1, in a reference frame where the flame is stationary, temperature (and other properties) is a function of position. The flame thickness δ_f and flame speed S_f are functions of the diffusive transport and the energy release due to chemical reactions.

Model. On length scales where the hydrodynamic effects are dominant, the problem can be simplified by neglecting dissipative effects and treating the flame as infinitely thin. The

reaction then becomes: Reactants $\Longrightarrow$ Products. The reaction is irreversible and the flame is modelled as a discontinuity which converts reactants to products and releases chemical energy equal to the heat of reaction. With this assumption, the problem is reduced to solving the one-dimensional compressible flow equations with an additional conserved scalar equation for the chemical energy. For simplicity, the ratio of specific heats is constant across the flame.

Compressible flow equations.

$$\frac{\partial \vec{U}}{\partial t} + \frac{\partial \vec{F}}{\partial x} = 0, \tag{1}$$

$$\vec{U} = \begin{bmatrix} \rho \\ \rho u \\ \rho E \end{bmatrix}, \qquad \vec{F} = \begin{bmatrix} \rho u \\ \rho u^2 + P \\ \rho u E + u P \end{bmatrix}. \tag{2}$$

$$E = e + q + \frac{u^2}{2}. \tag{3}$$

Chemical energy equation.

$$\frac{\partial}{\partial t}(\rho q) + \frac{\partial}{\partial x}(\rho u q) = 0. \tag{4}$$

Equation of state.

$$P = (\gamma - 1)\rho e. \tag{5}$$

The symbols are defined in the Appendix. While the chemical energy is a conserved scalar on either side of the combustion wave, its value is changed at the flame front as energy is converted from chemical energy to internal and kinetic energy.

Rankine–Hugoniot relations. Consider the hyperbolic system of equations that describes the current system. For an arbitrary surface of discontinuity in a flow field, the fluxes of conserved quantities must be equal entering and leaving. Stated more formally, for a system of equations of the form given by (1), and a discontinuity travelling at speed, s, one can write $s[U_i] = [F_i]$ where $[U_i] \equiv U_{i,L} - U_{i,R}$ is defined as the jump in the ith element of vector U across the discontinuity. These equations are called the Rankine–Hugoniot relations and in this system represent the conservation of mass, momentum, and energy.

Detonations versus deflagrations. There are two types of combustion waves of interest in this model: weak deflagrations and strong (or in the limit, Chapman–Jouguet (CJ)) detonations. We exclude the possibilities of weak detonations and strong deflagrations based on both physical (see [18]) and mathematical arguments (see [12], [15]). The relation of the characteristic directions to the trajectory of the reaction front determines whether a unique solution exists (see [15]). For a strong detonation the characteristic directions are similar to the case for a nonreacting shock (Fig. 2). A counting argument can be used to illustrate the uniqueness of the solution.

The detonation is a discontinuity separating two known smooth states $U_L(x, t)$ and $U_R(x, t)$. At some short time later δt we are interested in finding the states on either side of the detonation $U_L(x_f(t + \delta t), t + \delta t)$ and $U_R(x_f(t + \delta t), t + \delta t)$ and the detonation speed $s(t + \delta t)$ where the position of the discontinuity is denoted by x_f. The jump in chemical energy Δq is specified, so we are left with seven unknown quantities. The Rankine–Hugoniot

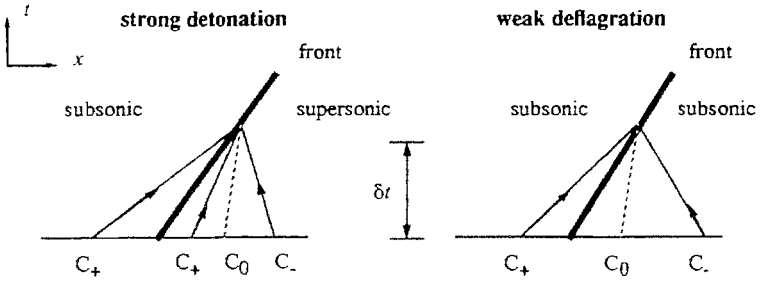

FIG. 2. *Relation between characteristic directions and the path of the reaction front. Strong detonation case, like that for a shock, is completely determined. The weak deflagration case has one degree of indeterminacy.*

relations provide three equations and for a strong detonation the information carried along the four characteristic directions intersecting the detonation provide four additional equations which uniquely determine the solution. For a CJ detonation, in addition to the three Rankine–Hugoniot relations, three characteristics intersect the discontinuity from the left and the CJ detonation propagates at the speed of sound. We have

$$s[U_i] = [F_i], \qquad i = 1, 2, 3,$$

(6)
$$\text{for strong detonations:} \quad l^k \cdot \frac{dU}{d\sigma^k} = 0, \qquad k = +R, -R, 0R, +L,$$

$$\text{for CJ detonations:} \quad l^k \cdot \frac{dU}{d\sigma^k} = 0, \qquad k = +R, -R, 0R,$$
$$s = u_L + c_L.$$

The equations describing the behavior of the solution along characteristics imply that the part of the vector U picked out by the kth left eigenvector l^k does not change along the kth characteristic trajectory σ^k. "L" and "R" indicate whether the characteristic approaches the discontinuity from the left or the right.

In contrast to the unique solution in the detonation case, a weak deflagration has one degree of indeterminacy. Again, we are interested in determining seven unknown quantities. The Rankine–Hugoniot relations provide three equations and the intersection of three characteristics ($+L, -R, 0R$) with the deflagration provide three additional equations; one more equation is needed to uniquely determine the solution. In this case, we specify the speed of the flame, relative to the fluid velocity, to remove the indeterminacy and close the system. For laminar combustion, the flame speed is determined primarily by the balance of the effects of chemical energy release and diffusive transport on length and time scales that are small relative to the hydrodynamic scales. In principle, the flame speed in that regime could be computed by solving a two-point boundary value problem for the traveling wave solution of the compressible Navier–Stokes equations. In the case of turbulent combustion, the flame is no longer one dimensional, but can be modeled as such in a quasi-one-dimensional approximation. In both regimes, it has been found that the flame speed can be parameterized as a power law function of the temperature of the fluid immediately in front of the flame (see [1], [2], [20], [23]). We have

(7)
$$S_f = u_0 + k\left(\frac{P_0}{\rho_0}\right)^Q.$$

Here, the values of k and Q are determined by fitting them to experimental flame speed data.

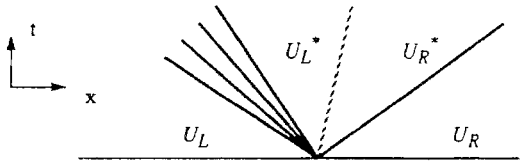

FIG. 3. *Gas dynamics Riemann solution: Shock tube.*

3. Solution procedure. The solution procedure utilizes the front tracking method of Chern and Colella [9] and the Riemann problem solution of Teng, Chorin, and Liu [23], [10]. A summary of the basic techniques is presented here. For more details, one should consult the original works.

Riemann problem solution. In order to implement the front tracking algorithm we need to calculate the speed of the tracked front and the fluxes passing through it. It is in this context that the solution to the Riemann problem must be discussed. In general, one is given a hyperbolic system of equations with initial data of the form given by (8). We are interested in finding the solution at later times. We have

$$\frac{\partial U}{\partial t} + \frac{\partial F}{\partial x} = 0, \tag{8}$$

$$U(x,0) = \begin{cases} U_L, & x < 0, \\ U_R, & x > 0. \end{cases}$$

Gas dynamics. The solution to the Riemann problem is well known for the gas dynamics equations [3×3 system]. We will use this example to illustrate some of the ideas involved in solving the general Riemann problem. Differences introduced in the case of reacting gas dynamics will then be discussed.

The solution to the gas dynamics Riemann problem consists of three waves: a left-moving gas wave, a right-moving gas wave, and a contact discontinuity travelling at the local fluid velocity. The gas waves can be either shocks or centered rarefactions. A typical solution for a shock tube is shown in Fig. 3.

First, consider shocks. For a known right state U_1 and pressure behind the shock $P_2 > P_1$, the state behind the shock is completely determined through the Rankine–Hugoniot jump conditions. For $\overline{P} = (P_1 + P_2)/2$, $\tau = 1/\rho$,

$$\begin{aligned} [u] &= W[\tau], \\ [P] &= -W^2[\tau], \\ [e] &= -\overline{P}[\tau], \end{aligned} \tag{9}$$

$$W^2 = \frac{\gamma P_1}{\tau_1}\left(1 + \frac{(\gamma+1)}{2\gamma}\frac{(P_2 - P_1)}{P_1}\right).$$

The Rankine–Hugoniot jump conditions represent conservation of mass, momentum, and energy across the discontinuity. If we view u_2, ρ_2 and the shock speed $s = u_1 + W\tau_1$ as the unknowns, then the jump conditions provide the three equations necessary to solve the system.

Now consider rarefactions. For a known right state U_1 and pressure behind the rarefaction $P_2 < P_1$, the state behind the rarefaction is determined by the equations of isentropic gas dynamics. In particular, for a γ-law gas, the Γ^- Riemann invariant is constant.

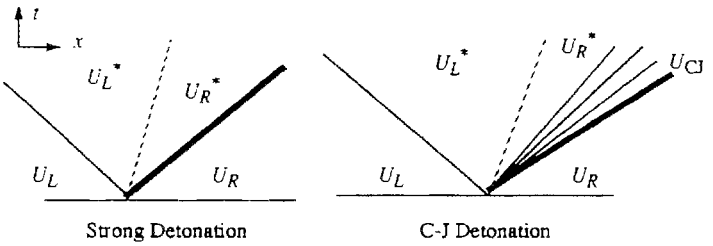

FIG. 4. *Detonation Riemann solution.*

$$\Gamma^- = u_1 - \frac{2c_1}{\gamma - 1} = u_2 - \frac{2c_2}{\gamma - 1},$$

$$P_2\rho_2^{-\gamma} = P_1\rho_1^{-\gamma}, \tag{10}$$

$$c = \sqrt{\gamma \frac{P}{\rho}}.$$

Thus, the velocity and density behind a rarefaction can be determined uniquely.

The solution to the gas dynamics Riemann problem is found by employing the fact that velocity and pressure are continuous across a contact discontinuity. First, guess the pressure between the two gas waves P^*. Determine whether the left and right waves are shocks or rarefactions and calculate the velocity using either (9) or (10). Pressure is iterated on until the velocities match across the contact discontinuity: $u_L^* = u_R^*$.

Reacting gas dynamics. The Riemann problem for reacting gas dynamics is more complex. Consider a reacting front separating two constant states with one side burned; the other is unburned. In the detonation case, a unique solution exists. However, for deflagrations whose velocity is specified by a given flame speed law, in addition to the detonation solution, there may be zero, one, or more than one solution involving a deflagration. We resolve this ambiguity by choosing the weakest combustion wave (in terms of pressure jump) that satisfies the conservation conditions.

In the detonation case, the solution to the Riemann problem is similar to that for the nonreacting gas dynamics (see Fig. 4). For a strong detonation $P_R^* > P_{CJ}$, the CJ detonation pressure, we see a right-moving detonation, a left-moving gas wave, and a contact discontinuity. We use the Rankine–Hugoniot jump conditions across the detonation in a similar manner to the treatment of a shock for the gas dynamics case. The jump conditions now contain information about the chemical energy as well:

$$[q] = \Delta H_R, \tag{11}$$

where ΔH_R is the heat of reaction.

For a CJ detonation $P_R < P_{CJ}$, the pressure at the detonation is known ($P = P_{CJ}$), and a rarefaction fan connects the detonation to U_R^*. The state behind the left gas wave is calculated as in the nonreactive case and the contact discontinuity provides the matching condition that closes the system. Again, guess P^* and iterate until $u_R^* = u_L^*$. The front speed is calculated as part of the Riemann solution. The reduced flux, needed for the tracking algorithm, is based on the state ahead of the detonation $F_f = F(U_R) - sU_R$.

The deflagration case is more complicated because it consists of four waves: left and right gas waves, a contact discontinuity, and a deflagration. The speed of the deflagration

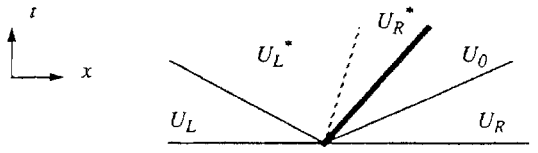

FIG. 5. *Deflagration Riemann solution.*

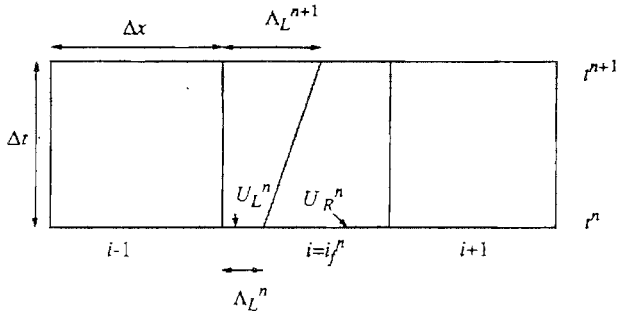

FIG. 6. *Tracked front.*

must be specified by a flame speed law, e.g., (7). A typical solution is presented in Fig. 5. The pressure in front of the deflagration P_0 is guessed and the solution is again iterative. The gas waves are dealt with in the usual way with the deflagration treated using Rankine–Hugoniot jump conditions for the specified flame speed. The difficulty occurs due to the possibility of more than one solution or no solution at all. The iteration is designed such that it picks out the weakest deflagration wave when multiple solutions exist. In the event that no solution containing a deflagration can be found, a detonation is assumed to exist. The information provided to the front tracking algorithm consists of the flame speed and the reduced flux $F_f = F(U_0) - sU_0$.

Front tracking. The strategy of front tracking is to treat a discontinuity as an internal boundary in the flow field using the solution to the Riemann problem to determine its speed and the fluxes passing through it. A conservative update of the solution is then performed. In order to maintain numerical stability near the tracked front as fractional cell size gets arbitrarily small, incremental values of the conserved quantities are redistributed according to the method of characteristics. Fig. 6 illustrates the finite difference cells in the neighborhood of the tracked front.

The location of the front at time $n\Delta t$ is denoted by x_f^n and the cell containing the front is labelled i_f^n. The solution at time $n\Delta t$ is known. The procedure for advancing the solution in time consists of the following steps:

1. Compute fluxes using a finite difference method for all cells in the domain. We will employ a second-order Godunov algorithm to calculate the fluxes (see [13], [14]). The numerical flux is a function of the solution in nearby cells. For stencil width r,

$$F_{i+\frac{1}{2}} = F(U_{i-r}^n, \ldots, U_{i+r}^n). \tag{12}$$

In the case that an edge is within r cell lengths of the tracked front, the values of the arguments of $F_{i+1/2}$ corresponding to cells on the opposite side of the tracked front are evaluated using the value U_L^n. In particular, we do not mix burned and unburned values in computing fluxes at cell edges. For edges to the right of the front, we use U_R^n to fill in the missing arguments of the flux function.

2. Update interior cells. For cells not in the neighborhood of the front (i.e., $i = 1 \ldots i_f^n - 2, i_f^n + 2 \ldots N$, where N is the number of cells in the domain), perform a conservative update of the solution.

$$U_i^{n+1} = U_i^n + \frac{\Delta t}{\Delta x}\left(F_{i-\frac{1}{2}} - F_{i+\frac{1}{2}}\right). \tag{13}$$

3. Update the front position. Calculate the representative left and right states

$$\overline{U}_L = U_L^n \frac{\Lambda_L^n}{\Delta x} + U_{i_{f,n}-1}^n \left(1 - \frac{\Lambda_L^n}{\Delta x}\right). \tag{14}$$

We compute $\overline{U}_R$ similarly. We use these values to calculate the solution to the Riemann problem determining the speed of the front s and the flux through the front $F^f = F(U) - sU$. This will be described in more detail in the next section.

Move the front

$$x_f^{n+1} = x_f^n + s\Delta t. \tag{15}$$

4. Make a first pass at updating the solution near the front. Define

$$\begin{aligned} \delta M_L &= (\Lambda_L^n - \Lambda_L^{n+1})U_L^n + \Delta t\left(F_{i_{f,n}-\frac{1}{2}} - F^f\right), \\ \delta M_R &= (\Lambda_R^n - \Lambda_R^{n+1})U_R^n + \Delta t\left(F^f - F_{i_{f,n}+\frac{1}{2}}\right). \end{aligned} \tag{16}$$

δM is defined such that the conservative update formula for U_L and U_R is

$$\begin{aligned} \Lambda_S^{n+1}U_S^{n+1} &= \Lambda_S^{n+1}U_S^n + \delta M_S, \\ S &= L, R. \end{aligned} \tag{17}$$

Note that this equation is unstable for a Courant–Friedrichs–Lewy (CFL) condition based on Δx since Λ_S^{n+1} can become arbitrarily small. We break δM into two parts in order to update the solution in a way that is both conservative and stable.

$$\delta M_S = \frac{\Lambda_S^{n+1}}{\Delta x}\delta M_S + \left(1 - \frac{\Lambda_S^{n+1}}{\Delta x}\right)\delta M_S = \delta M_{S,1} + \delta M_{S,2}. \tag{18}$$

δM_1 can be added to update the solution in a stable manner

$$U_S^{n+1} = U_S^n + \frac{1}{\Lambda_S^{n+1}}\delta M_{S,1} = U_S^n + \frac{1}{\Delta x}\delta M_S. \tag{19}$$

5. Redistribute $\delta M_{S,2}$ in cells near the front to maintain conservation. The general procedure is to perform an eigenvalue decomposition of the vector $\delta M_{S,2}$. The parts are distributed to where they would be propagated according to the method of characteristics. There is an important difference in the treatment of combustion waves, however, where we assume the characteristics starting from the left of the front (burned side) reflect off the front so that distribution of conserved quantities corresponding to these parts occurs only in the burned region. This is essential to insure both that fuel is not burned twice and that the unburned state contains no burned gas. We allow characteristics to cross the flame from the right (unburned side), corresponding to fuel being consumed slightly before it normally would. Algebraically, this is expressed

$$\delta M_{S,2} = \sum_k \alpha_S^k r_S^k. \tag{20}$$

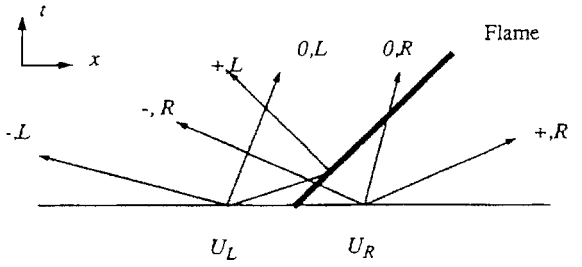

FIG. 7. *Characteristics for flame problem (deflagration).*

where

$$\begin{aligned} \alpha_S^k &= l_S^k \cdot \delta M_{S,2}, \\ r_S^k &= r^k(\overline{U_S}), \\ l_S^k &= l^k(\overline{U_S}), \\ k &= -, 0\rho, 0q, +. \end{aligned}$$

where r^k and l^k are the kth right and left eigenvectors and α^k is the corresponding expansion coefficient. The propagation of the components are determined by the eigenvalues λ^k. Notice there are four eigenvectors for this system: two travel at the fluid velocity, carrying jumps in density and chemical energy. For this system, the left and right eigenvectors are

$$\begin{aligned} l^{\pm} &= \frac{1}{2}\left[\frac{1}{\gamma} \mp \frac{u}{c} + \left(\frac{u^2+q-E}{e\gamma}\right), -\left(\frac{u}{e\gamma} \mp \frac{1}{c}\right), \frac{1}{e\gamma}, -\frac{1}{e\gamma}\right], \\ l^{0\rho} &= \frac{1}{e\gamma}\left[\frac{P}{\rho} - (u^2+q-E), u, -1, 1\right], \\ l^{0q} &= \left[-\frac{q}{\rho}, 0, 0, \frac{1}{\rho}\right]. \end{aligned} \tag{21}$$

$$\begin{aligned} r^{\pm} &= \left[1, u \pm c, E \pm \frac{P}{\rho}, q\right]^T, \\ r^{0\rho} &= [1, u, E-e, q]^T, \\ r^{0q} &= [0, 0, \rho, \rho]^T. \end{aligned} \tag{22}$$

and $\lambda^{\pm} = u \pm c$, $\lambda^{0\rho,0q} = u$.

The part of $\delta M_{S,2}$ that is carried by each characteristic is defined:

$$\delta M_S^k = \alpha_S^k r_S^k. \tag{23}$$

In the case of a deflagration front, we represent the redistribution process by the characteristic diagram in Fig. 7. Note that the $+, L$ characteristic is reflected back into the burned region as discussed above.

We define δM_L^{tot} and δM_R^{tot} for redistribution behind and in front of the discontinuity:

$$\begin{aligned} \delta M_R^{\text{tot}} &= \delta M_R^+, \\ \delta M_L^{\text{tot}} &= \delta M_L^- + \delta M_L^{0\rho} + \delta M_L^{0q} + \delta M_L^+ + \delta M_R^- + \delta M_R^{0\rho} + \delta M_R^{0q}. \end{aligned} \tag{24}$$

We then distribute these quantities near the front:

$$
\begin{aligned}
U^{n+1}_{i_{f,n+1}+1} &:= \left(U^{n+1}_{i_{f,n+1}+1} + \frac{1}{\Lambda^{\text{tot}}_R}\delta M^{\text{tot}}_R\right),\\
U^{n+1}_{R} &:= \left(U^{n+1}_{R} + \frac{1}{\Lambda^{\text{tot}}_R}\delta M^{\text{tot}}_R\right),\\
U^{n+1}_{i_{f,n+1}-1} &:= \left(U^{n+1}_{i_{f,n+1}-1} + \frac{1}{\Lambda^{\text{tot}}_L}\delta M^{\text{tot}}_L\right),\\
U^{n+1}_{L} &:= \left(U^{n+1}_{L} + \frac{1}{\Lambda^{\text{tot}}_L}\delta M^{\text{tot}}_L\right),
\end{aligned}
\tag{25}
$$

where

$$
\begin{aligned}
\Lambda^{\text{tot}}_R &= \Lambda^{n+1}_R + \Delta x,\\
\Lambda^{\text{tot}}_L &= \Lambda^{n+1}_L + \Delta x,
\end{aligned}
\tag{26}
$$

and ":=" in (25) represents assignment in place. A similar calculation is performed in the detonation case, except that all four characteristics cross from unburned to burned.

$$
\begin{aligned}
\delta M^{\text{tot}}_L &= \delta M^{-}_L + \delta M^{0\rho}_L + \delta M^{0q}_L + \delta M^{+}_L + \delta M^{-}_R + \delta M^{0\rho}_R + \delta M^{0q}_R + \delta M^{+}_R,\\
\delta M^{\text{tot}}_R &= 0.
\end{aligned}
\tag{27}
$$

4. Results and discussion. The front tracking algorithm has been implemented for solving one-dimensional reacting gas flow problems. Results are shown in Figs. 8–11 for two different sets of flame speed constants. For each case the initial data represents an ignition problem.

Deflagration. First consider the deflagration problem (Figs. 8–9) on the domain [0, 1.6]. A solid wall exists at $x = 0$, allowing gas waves to reflect off of it. The boundary at the other end is open. We use 800 grid points in the x-direction ($\Delta x = 2.0e-3$) and the time step is determined by the CFL stability condition ($\Delta t = 0.9|\max(|u+c|, |u-c|)$). The initial data is

- unburned ($x < 0.075$ and $x > 0.081$): $P(x,0) = 1.0$; $\rho(x,0) = 1.0$; $q(x,0) = 20.0$; $u(x,0) = 0.0$.
- burned ($0.075 < x < 0.081$): $P(x,0) = 1.4072$; $\rho(x,0) = 0.2082$; $q(x,0) = 0.0$; $u(x,0) = 0.0$.

The flame speed constants are $k = 0.095$ and $Q = 2.0$. The burned state, obtained from the Riemann solution, is found behind a deflagration given left and right states equal to the unburned state above. The velocity is set to zero, however, since at early times we assume the effects of the left and right flame cancel.

The behavior of the system is shown at early times in Fig. 9 to illustrate the interaction of the hydrodynamics with the deflagration. Shock waves are labelled "s"; deflagration waves, "f." We first see two deflagrations propagating in opposite directions, each preceded by a shock wave. A short time later, the left-moving shock reflects off the closed end of the tube and decelerates the flame when the two waves collide (point D). The shock passes through the left flame and overtakes the right-moving flame causing the right-moving flame to accelerate (point A). It is this process of shock waves overtaking the right-moving flame and causing an increase in pressure that results in transition to detonation in this model. For the present flame speed constants, however, transition is not observed. Figure 8 shows the temperature contours for this problem at longer times.

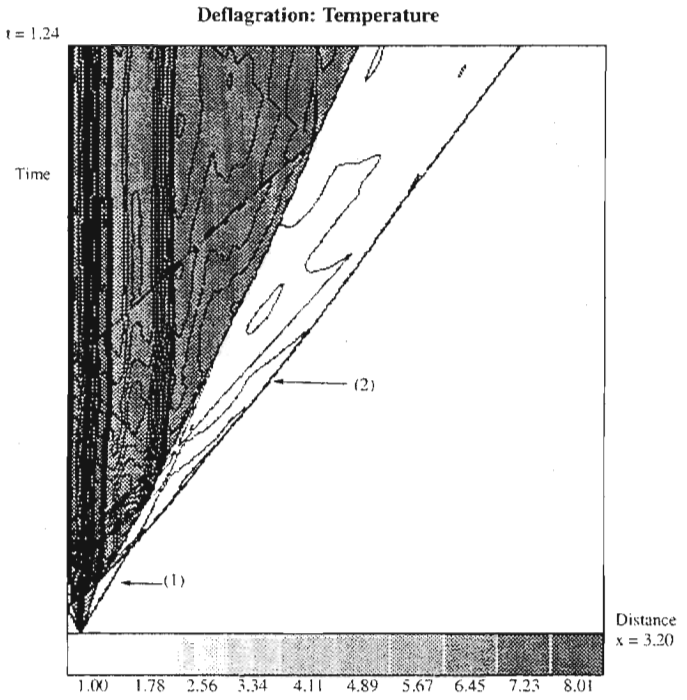

FIG. 8. *Temperature contours for* $k = 0.095$, $Q = 2$. (1) *and* (2) *denote the location of pressure cross sections shown in Fig. 12.*

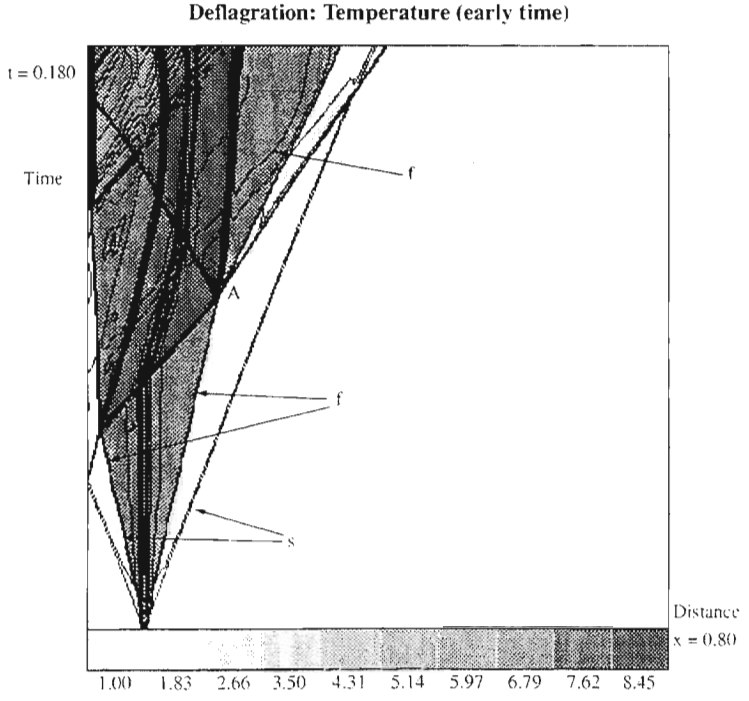

FIG. 9. *Early time behavior for* $k = 0.095$, $Q = 2$. *Temperature contours. Point* D *marks deceleration of the left flame. Point* A *marks acceleration of the right flame.*

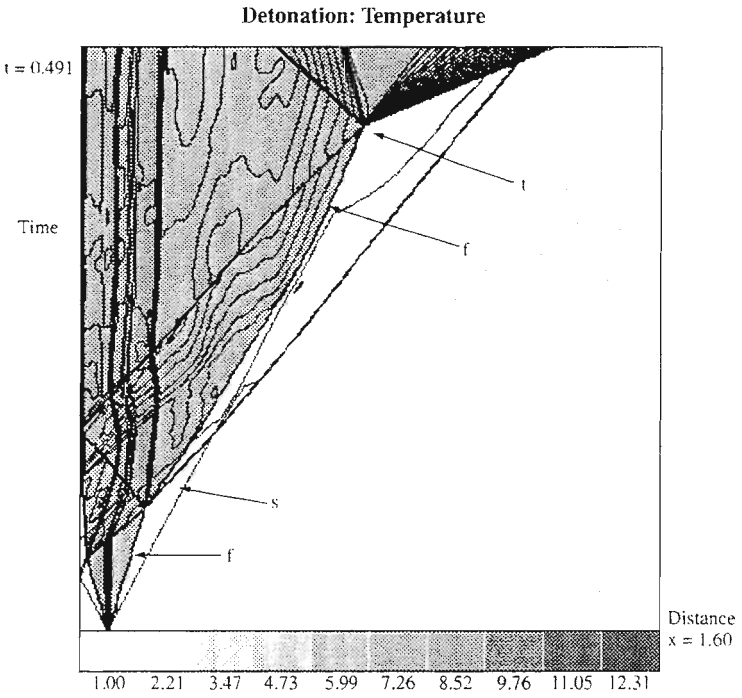

FIG. 10. *Temperature contours for* $k = 0.10$. $Q = 2$. *Transition to detonation occurs at point* t. "s" *indicates a shock*; "f" *indicates a flame.*

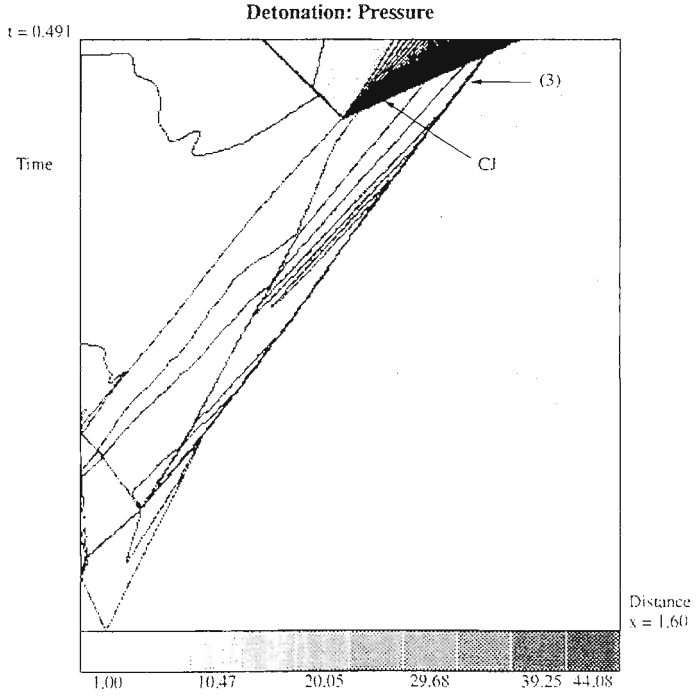

FIG. 11. *Pressure contours for* $k = 0.10$. $Q = 2$. *Note the strong rarefaction fan trailing the* CJ *detonation.* (3) *denotes the location of a pressure cross section shown in Fig. 12.*

Detonation. For the detonation problem, we consider a smaller domain [0, 1.6] since the phenomenon of interest occurs relatively quickly. We again use 800 grid points ($\Delta x = 2.0e-3$) and the CFL condition determines the time-step size. The initial data is

- unburned ($x < 0.075$ and $x > 0.081$): $P(x,0) = 1.0$; $\rho(x,0) = 1.0$; $q(x,0) = 20.0$; $u(x,0) = 0.0$.
- burned ($0.075 < x < 0.081$): $P(x,0) = 1.5075$; $\rho(x,0) = 0.2233$; $q(x,0) = 0.0$; $u(x,O) = 0.0$.

The flame speed constants are $k = 0.10$ and $Q = 2.0$. The burned state is obtained from the Riemann solution with the current configuration. We track two opposite-moving combustion waves.

The early time behavior of the present case (Figs. 10–11) is similar to that seen in Fig. 9. The left-moving shock reflects off the closed end of the tube and overtakes the right-moving deflagration. The right combustion wave accelerates, but is still a deflagration. Another shock overtakes the right-moving deflagration at point "t" and transition to detonation occurs. The detonation travels faster than the local speed of sound and the strong rarefaction fan trailing it indicates that it is a CJ detonation.

Figure 12 presents cross sections in time of the pressure field. The approximate location of these cross sections is shown in Fig. 8 for the deflagration cases (1) and (2) and in Fig. 11 for the detonation case (3). Note the different scales. Graph 12(1) illustrates the pressure field at early times. There is a substantial increase in pressure behind the shock and a slight decrease in pressure across the flame. At later times (2), we see a fairly strong shock at $x \approx 1.0$ followed by a rarefaction fan. A second weaker shock precedes the flame creating a small jump in pressure. The sharp pressure decrease at $x \approx 0.7$ marks the flame. The detonation pressure field (3) is significantly different. We see a shock wave at $x \approx 1.15$ followed by a CJ detonation producing an order of magnitude jump in pressure. A rapid expansion follows the detonation.

5. Accuracy. We have analyzed the accuracy of the numerical scheme in a number of ways. The most obvious of these compares the computed solution for an unsupported CJ detonation to its known analytical solution. Thus, we compute

$$\|U_h - U_{\text{exact}}\|_{L_1} / \|U_{\text{exact}}\|_{L_1} \tag{28}$$

for two values of $h(= \Delta x, \Delta x/2)$. The convergence rate is found by comparing the solution from successively refined grids. The scheme is evaluated for two sets of initial data:

$$\vec{U}(x,0) = \begin{cases} \vec{U}_R, & x > x_{\text{front}}, \\ \vec{U}_{\text{CJ}}(\vec{U}_R), & x < x_{\text{front}}, \end{cases} \quad \text{Discontinuous,} \tag{29}$$

$$\vec{U}(x,0) = \vec{U}(x, 0.01), \quad \text{all } x, \quad \text{Continuous.}$$

As shown in Table 1, for discontinuous initial data we observe first-order accuracy for the scheme. This is to be expected since the finite difference scheme will resolve discontinuities to first order at best. For initial data obtained from the analytical solution at an early time, the numerical result is better than second-order accurate. The algorithm is designed such that for tracked waves with constant states on both sides of the front, the calculated front position is exactly equal to the analytical result.

In an effort to determine the accuracy of the algorithm for more complex problems, we examine the convergence of both the front location and overall solution as the grid is refined. A classical convergence study is performed on the overall solution. The norm of the error is calculated by comparing data from successively refined grids: $\Delta x = 1/n$ for

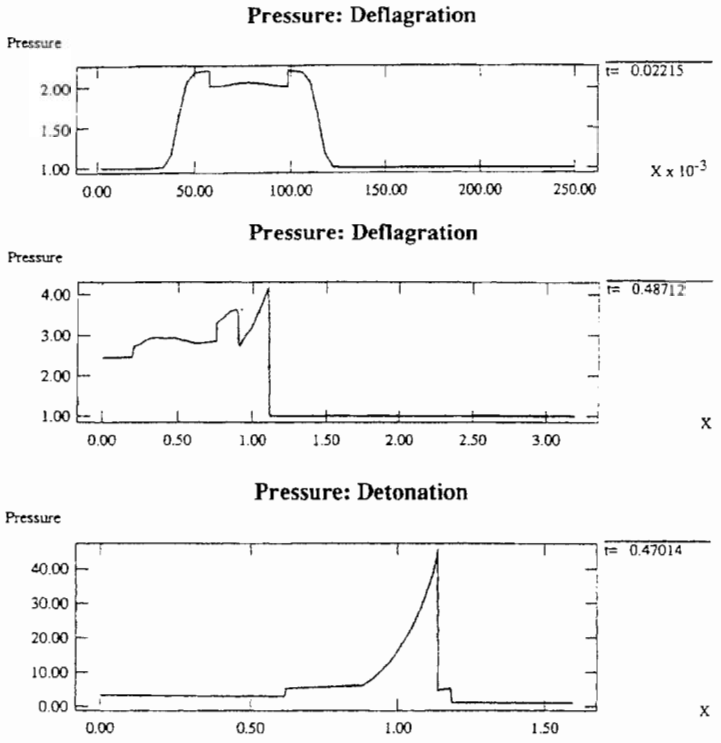

FIG. 12. *Pressure field (top to bottom). (1) early time deflagration; (2) late time deflagration; (3) CJ detonation.*

TABLE 1
Accuracy relative to known solution—CJ detonation.

Initial data	400-exact	800-exact	L_1 rate
Discontinuous	1.612E-3	7.724E-4	1.06
Continuous	2.206E-5	3.431E-6	2.68

$n = 200, 400, 800, 1600, 3200$. A small time step $\Delta t = 0.08\Delta x$ is used to insure stability as reflected shocks increase the sound speed. Thus, we compute

$$\frac{\left\| U_{h/2}^{avg} - U_h \right\|_{L_1}}{\| U_h \|_{L_1}} \tag{30}$$

for each grid. Asymptotically, these differences are proportional to the errors on the coarser grid. We evaluate the convergence for a test problem similar to the deflagration case examined in §4. The same initial states are used with the two front locations arranged to insure that at least one cell exists between the tracked fronts for the coarsest grid: $x_{f,L} = 0.1175$, $x_{f,R} = 0.1275$.

The accuracy is checked at an early time $t = 0.12$ before the flame is overtaken by a reflected shock and at a later time $t = 0.32$ after the reflected shock has passed through the flame (Figs. 13 and 14). At both times, the solution is converging at a rate slower than first order, a reasonable result given the complexity of the problem (Table 2). The data in the 200 cell case is not in the asymptotic region and therefore the 0.209 convergence rate is most likely an anomaly.

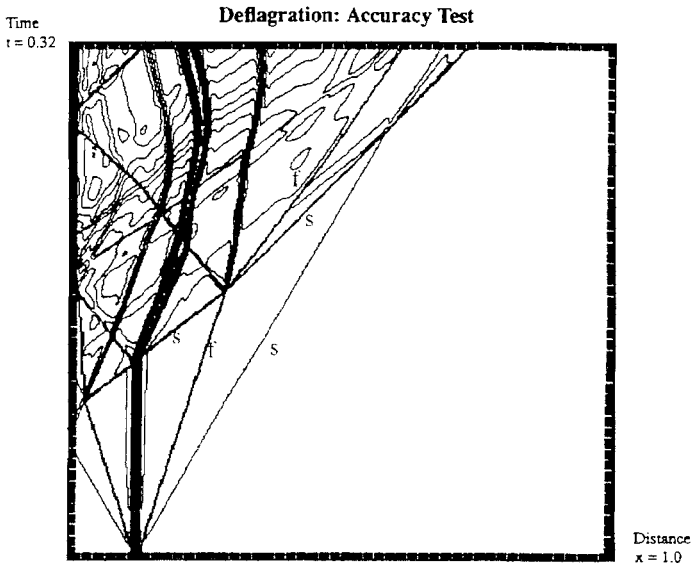

FIG. 13. *Density contour plot for accuracy test problem. At* $t \approx 0.17$, *shock overtakes the flame. Error is evaluated at* $t = 0.12$ *and* $t = 0.32$. *"f" marks right moving flame; "s" indicates shock.*

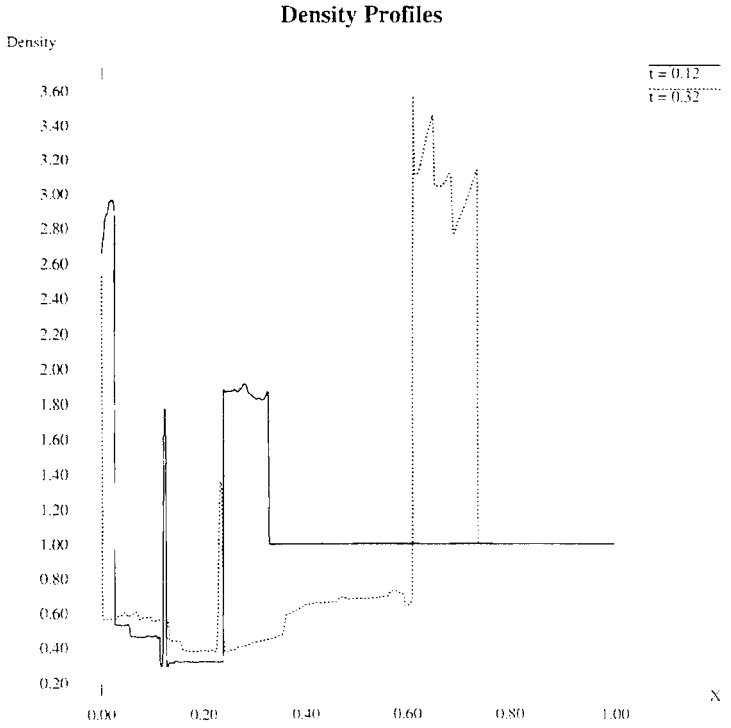

FIG. 14. *Density profiles at* $t = 0.12$ *and* $t = 0.32$ *for accuracy test problem. For* $t = 0.12$, *the left-moving flame is located at* $x \cong 0.02$; *the right-moving flame at* $x \cong 0.24$. *At* $t = 0.32$, *the right flame is located at* $x \cong 0.60$.

TABLE 2
Error for deflagration in a complex flow field.

Time	200–400	Rate	400–800	Rate	800–1600	Rate	1600–3200
$t = 0.12$	6.88E-3	0.209	5.95E-3	0.722	3.61E-3	0.561	2.44E-3
$t = 0.32$	7.53E-2	0.671	4.73E-2	0.869	2.59E-2	0.665	1.63E-2

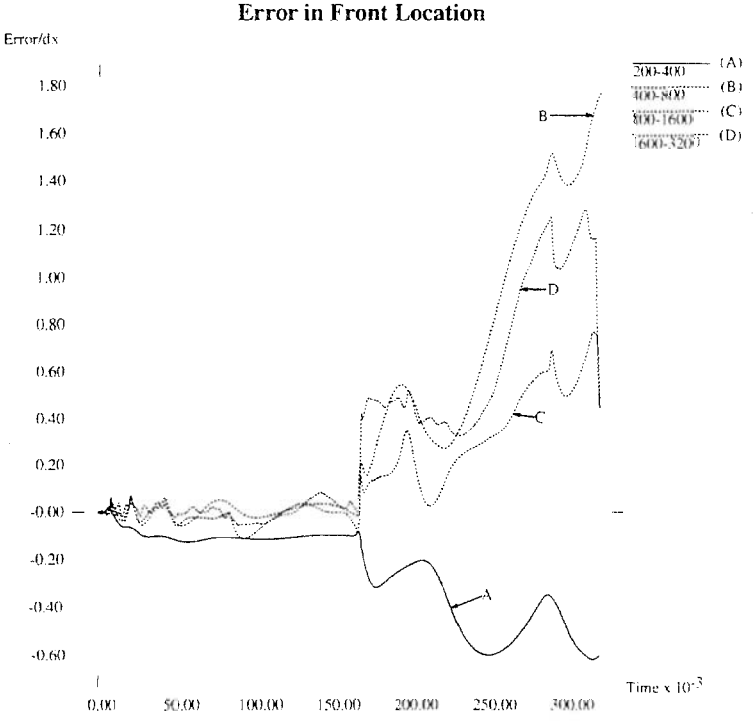

FIG. 15. *Error in front location scaled by Δx. Note that before shock overtakes flame at $t \cong 0.17$, the error is an order of magnitude smaller than Δx. Also, observe the oscillatory behavior of the error.*

The convergence of the front location (right-moving flame) is also examined (Fig. 15). We plot $(x_{f,n} - x_{f,2n})/(\Delta x_n)$ for times when $x_{f,n}$ is defined. For short times corresponding to the first case above, the error in the front location is an order of magnitude smaller than the grid spacing. After the shock passes through the flame at $t \approx 1.6$, the error increases but still is on the order of one grid cell. One should note the oscillatory behavior of the error. This may be due to the corrective effect of the tracking algorithm: as mass and energy are redistributed behind the flame a local high energy region is created causing an increase in front speed. The bulk states near the flame cannot support that speed so the flame speed decreases until a local low energy region is created and the process repeats in reverse. Further, it is this feature of the error that makes a classical convergence study of front location impossible. That is, while the error in the front position, on average, decreases with grid refinement, the error at a given time for successively refined grids does not monotonically go to zero. The oscillations have different amplitudes and frequency for each grid resulting in arbitrary cancellation of error. Again note that these errors are small (Fig. 16).

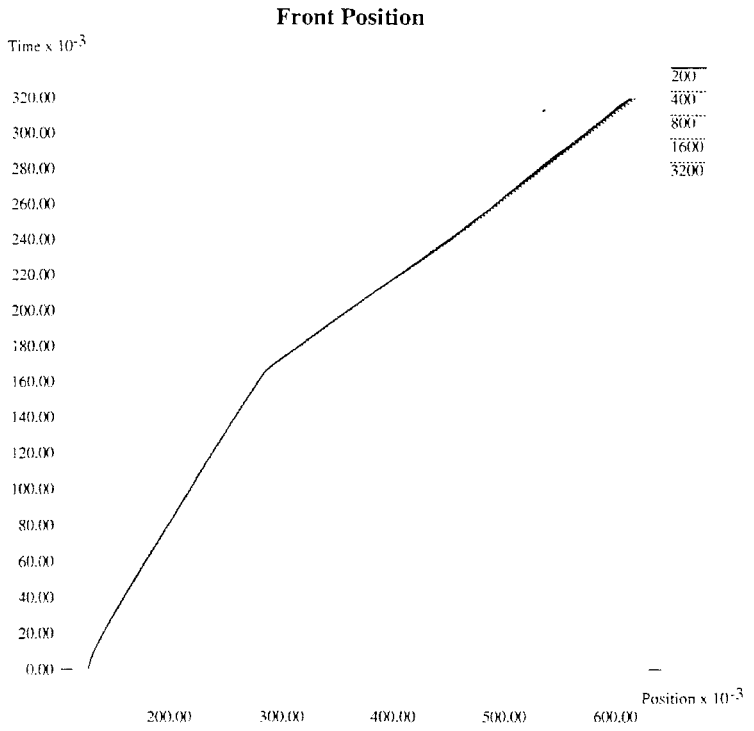

FIG. 16. *Front location versus time. Error in the front position is on the order of the grid spacing.*

6. Conclusions. We have looked at the front tracking method applied to one-dimensional reacting gas flow. The results accurately represent the interaction of gas dynamics waves with detonations and deflagrations that can be modelled by flame laws of a form similar to (7). The current method produces results that are qualitatively similar to the results that Teng, Chorin, and Liu [23] obtained using a different numerical method. The present work has the advantage that it can be generalized to more than one dimension and has the potential to include adaptive mesh numerical techniques. Such extensions will be investigated in future work.

REFERENCES

[1] G. E. ANDREWS AND D. BRADLEY, *The burning velocity of methane-air mixtures*, Combustion and Flame, 19 (1972), pp. 222–238.

[2] ———, *Determination of burning velocity by double ignition in a closed vessel*, Combustion and Flame, 20 (1973), pp. 77–89.

[3] J. BDZIL AND D. S. STEWART, *Modeling two-dimensional detonations with detonation shock dynamics*, Phys. Fluids A, 1 (1989), pp. 1261–1270.

[4] J. B. BELL, P. COLELLA, AND M. WELCOME, *Conservative front tracking for inviscid compressible flow*, Proc., 10th AIAA Computational Fluid Dynamics Conference, Honolulu, HI, June 24–27, 1991, pp. 814–822.

[5] A. BOURLIOUX AND A. J. MAJDA, *Theoretical and numerical structure for unstable two-dimensional detonations*, Combustion and Flame, 90 (1992), pp. 211–229.

[6] B. BUKIET, *The effect of curvature on detonation speed*, SIAM J. Appl. Math., 49 (1989), pp. 1433–1446.

[7] ———, *Application of front tracking to two-dimensional curved detonation fronts*, SIAM J. Sci. Statist. Comput., 9 (1988), pp. 80–99.

[8] B. G. Bukiet and R. Menikoff, *Detonation waves and the front tracking method*, Phys. Fluids A, 4 (1992), pp. 2070–2081.

[9] I. L. Chern and P. Colella, *A conservative front tracking method for hyperbolic conservation laws*, Tech. report UCRL-97200, Lawrence Livermore National Laboratory, Livermore, CA, July, 1987.

[10] A. J. Chorin, *Random choice methods with applications to reacting gas flow*, J. Comput. Phys., 25 (1977), pp. 253–272.

[11] ———, *Flame advection and propagation algorithms*, J. Comput. Phys., 35 (1980), pp. 1–11.

[12] A. J. Chorin and J. E. Marsden, *A Mathematical Introduction to Fluid Mechanics*, 2nd ed., Springer-Verlag, New York, 1990.

[13] P. Colella, *Multidimensional upwind methods for hyperbolic conservation laws*, J. Comput. Phys., 87 (1990), pp. 171–200.

[14] P. Colella and P. R. Woodward, *The piecewise parabolic method (PPM) for gas dynamical simulations*, J. Comput. Phys., 54 (1984), pp. 174–201.

[15] R. Courant and K. O. Friedrichs, *Supersonic Flow and Shock Waves*, Interscience Publishers, Inc., New York, 1948.

[16] A. Ghoniem, A. J. Chorin, and A. K. Oppenheim, *Numerical modeling of turbulent flow in a combustion tunnel*, Trans. Roy. Soc. London, Ser. A, 304 (1982), pp. 303–331.

[17] J. M. Hyman, *Numerical methods for tracking interfaces*, Physica D, 12 (1985), pp. 396–407.

[18] K. K. Kuo, *Principles of Combustion*, John Wiley & Sons, New York, 1986.

[19] J. Kurylo, H. A. Dwyer, and A. K. Oppenheim, *Numerical analysis of flowfields generated by accelerating flames*, AIAA J., 18 (1979) p. 302.

[20] B. Lewis and G. von Elbe, *Combustion, Flames and Explosions of Gases*, 2nd ed., Academic Press, New York, 1961.

[21] R. Pember, J. B. Bell, P. Colella, W. Y. Crutchfield, and M. Welcome, *An adaptive cartesian mesh method for compressible flow in three dimensions*, Proc., 11th AIAA Computational Fluid Dynamics Conference, Orlando, FL, July 6–9, 1993.

[22] J. Sethian, *Turbulent combustion in open and closed vessels*, J. Comput. Phys., 54 (1984), pp. 425–456.

[23] Z.-H. Teng, A. J. Chorin, and T.-P. Liu, *Riemann problem for reacting gas, with applications to transition*, SIAM J. Appl. Math., 42 (1982), pp. 964–981.

[24] F. A. Williams, *Combustion Theory*, Addison–Wesley, Redwood City, CA, 1985.